Contents lists available at ScienceDirect

Materials Science & Engineering C
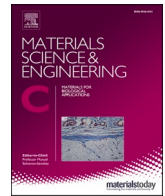
MiR-181d-5p regulates implant surface roughness-induced osteogenic differentiation of bone marrow stem cells

Yanping Liu [a], Yixiang Wang [b], Xian Cheng [c], Yan Zheng [a], Mingyue Lyu [a], Ping Di [a,*], Ye Lin [a,*]

[a] Department of Oral Implantology, Peking University School and Hospital of Stomatology, Beijing 100081, PR China
[b] Department of Central Laboratory, Peking University School and Hospital of Stomatology, Beijing 100081, PR China
[c] Department of Dentistry-Biomaterials, Radboud University Medical Center, Philips van Leydenlaan 25, 6525 EX Nijmegen, the Netherlands

ARTICLE INFO

ABSTRACT

Constructing moderate surface roughness is a widely used, non-toxic, cost-effective, and outcome-predictable approach to accelerate implant osteointegration in clinical settings. MicroRNAs (miRNAs) play vital regulatory roles in the osteogenic differentiation of bone marrow stem cells (BMSCs). However, their specific contribution to the influence of surface roughness on osteoblastic behavior remains unknown. Therefore, applying the smooth titanium surface as a control, a typical titanium surface with moderate roughness was prepared here to reveal the mechanism through which surface roughness regulates cell osteogenic behavior by altering miRNA expression. First, the morphology and roughness of two surfaces were characterized, and the enhanced osteogenic differentiation of BMSCs on rough surfaces was verified. Then, twenty-nine differentially expressed miRNAs in BMSCs cultured on different surfaces were selected via miRNA chip and corresponding functional prediction. After verifying the expression of these miRNAs using quantitative real-time polymerase chain reaction, four were considered eligible candidates. Among these, only miR-181d-5p significantly affected *RUNX2* gene expression based on overexpression and knockdown experiments. From the osteogenesis-related gene and protein expression, as well as alkaline phosphatase and alizarin red experiments, we further confirmed that the downregulation of miR-181d-5p promoted osteogenic differentiation of BMSCs, and vice versa. In addition, rescue assays showed that the knockdown of miR-181d-5p improved the inferior osteogenesis observed on smooth surfaces, whereas the overexpression of miR-181d-5p suppressed the superior osteogenesis observed on rough surfaces. These results indicate that the moderate surface roughness of the implant stimulates the osteogenic differentiation of BMSCs by remarkably downregulating miR-181d-5p. These findings provide helpful information and a theoretical basis for the development of advanced implant materials for fast osteointegration.

1. Introduction

Implants have been widely applied to various clinical disciplinary scenarios for bone repair, such as orthopedics (e.g. fracture fixation) [1], neurosurgery (e.g. closing skull bone defects) [2], otolaryngology (e.g. treatment of sensorineural hearing loss) [3], and dentistry (implant restoration of lost teeth) [4]. The clinical outcomes of these medical treatments are largely determined by the osseointegration status at the interface between implant surfaces and surrounding bone tissue [5,6]. The implant surface characteristics, such as surface chemistry, wettability, surface charge, and surface roughness, can be tailored through manifold approaches to affect the cell morphology, proliferation [7] and even guide the osteogenic differentiation of bone marrow stem cells (BMSCs) [8–11]. Compared with other implant surface modifications, constructing appropriate surface roughness has become one of the most widely used methods to accelerate implant osseointegration in the clinic currently, with advantages including non-toxicity, cost-effectiveness, and clinical outcome-predictability [12,13]. A systemic review summarized data indicating that implant surfaces with smooth (Sa < 0.5 μm) and minimal roughness (Sa 0.5–1 μm) result in less bone formation than rough surfaces, whereas surfaces with moderate roughness (Sa 1–2 μm) result in greater bone formation than extremely rough surfaces (Sa > 2 μm) [14]. Afterwards, implant surfaces with moderate roughness applied in medical practices were deemed optimal to promote

---

osteogenesis [14–17].

MicroRNAs (miRNAs) are a class of small non-coding RNAs that function in RNA silencing and modulating gene expression at the post-transcriptional stage by destabilizing target messenger RNAs or inhibiting protein translation [18,19]. Increasing evidence demonstrates that miRNAs have pivotal roles in the gene regulatory networks involved in the osteogenic differentiation of osteoblasts [20–22]. For example, miR-204 acts as an endogenous attenuator of *RUNX2* to negatively regulate the osteogenic differentiation and determine cell fate in BMSCs [20]. Hassan et al. reported that osteoblast differentiation is repressed by the exogenous expression of miRNA cluster 23a–27a–24-2, which was further inhibited by *RUNX2* [21]. Another recent study found that a random nano-fibrous alignment substrate can induce osteogenesis of BMSCs via the miR-193a-3p-MAP3k3 signaling axis [22]. However, little is known about the specific roles of miRNAs in implant surface roughness-induced osteogenic differentiation of BMSCs.

In this study, by using the smooth titanium surface as a control, a typical titanium implant surface with moderate roughness was prepared to reveal the mechanism through which surface roughness regulates osteoblastic behavior by altering miRNA expression. First, human bone marrow stem cells (hBMSCs) were cultured on two types of surfaces to observe the roughness-induced osteogenic differentiation. Then, a miRNA chip was adopted for the rapid screening of differentially expressed miRNAs in hBMSCs. The potential miRNAs were predicted from software according to gene targets in terms of osteogenic differentiation and cytoskeleton-related functions, and their expression levels were verified by quantitative real-time polymerase chain reaction (qPCR). Subsequently, overexpression and knockdown experiments of the eligible potential miRNAs were conducted to assess whether they could influence osteogenesis-related gene expression. After stepwise selection, the confirmed miRNA was overexpressed and knocked down to study its roles in regulating osteogenic differentiation of hBMSCs via qPCR, western blotting, alkaline phosphatase tests, and alizarin red tests. In addition, a rescue assay was performed to confirm the impact of the downregulation and overexpression of this miRNA on the osteogenic differentiation of hBMSCs on moderately rough or smooth surfaces.

2. Materials and methods

2.1. Surface preparation and characterization

Pure titanium (Ti) implant materials (grade 4) were used. The Ti stick was cut into slices of 1-mm thickness. The diameters of the slices were 15 mm for 24-well, 22 mm for 12-well, and 34 mm for 6-well plates. Each slice was ground with silicon carbide paper, cleaned ultrasonically three times in acetone, ethyl alcohol, and deionized water for 10 min, and air-dried. The slices were divided into two groups, moderately rough Ti implant surface (TiR) and machined smooth Ti implant surface (TiS). TiR surfaces were treated with sand-blasting and acid-etching involving large grit sandblasting, etching with a mixture of hydrofluoric acid and nitric acid, and washing ultrasonically in deionized water. The TiR and TiS surfaces were characterized via two methods. First, surface morphologies were qualitatively analyzed utilizing scanning electron microscopy (SEM; Hitachi-S3400N, Tokyo, Japan). Second, quantitative three-dimensional characteristics were analyzed based on roughness parameters (Sa: arithmetic mean deviation of the surface; Sq: root-mean-square deviation of the surfaces) determined using a 3D optical profiler (ContourGT-K0; Bruker, Billerica, MA, USA). Five images were examined for each surface.

2.2. Cell culture

hBMSCs were purchased from Cyagen (Santa Clara, CA, USA) and cultured in α-modified Eagle's medium (α-MEM; Gibco, Waltham, MA, USA) containing 10% fetal bovine serum (FBS; Gibco) and 1% penicillin/streptomycin at 37 °C in a humidified atmosphere with 5% CO_2.

The hBMSCs were then passaged using 0.25% trypsin after reaching 70–90% confluence, and passages 2–4 were expanded for subsequent experiments. The osteogenic induction medium was the aforementioned growth medium supplemented with 0.1 μM dexamethasone, 0.2 mM L-ascorbic acid, and 10 mM β-glycerophosphate (Sigma-Aldrich, St. Louis, MO, USA).

2.3. Cell morphology

The sterilized slices were placed in 24-well plates, and the hBMSCs were seeded on TiR and TiS surfaces at a cell density of 1×10^4 cells/cm^2. After incubation for 24 h, Immunofluorescence tests were performed to investigate the cell morphology. The cells were fixed with 4% paraformaldehyde for 30 min and permeabilized with 0.1% triton X-100 for 5 min. The nonspecific bonding sites were blocked with 1% bovine serum albumin (BSA) for 1 h. Then, the cells were immunostained with antibodies against F-actin (Sigma-Aldrich) for 1 h and counterstained with DAPI (Solarbio, Beijing, China) for 5 min. Fluorescent images were obtained using a confocal laser scanning microscope (LSM710, Carl Zeiss, Oberkochen, Germany). After incubation for 1, 3, and 7 days, the cell proliferation was estimated by the cell counting kit-8 (CCK-8, Dojindo Laboratories, Kumamoto, Japan) according to the manufacturer's protocol. To investigate the inhibition of cytoskeletal organization, 10 μM Y27632 (MedChemExpress, HJ, USA) was added to the culture medium. Then, hBMSCs with treatment were used for fluorescent staining and qPCR.

2.4. MiRNA microarray and gene prediction

Total RNA was harvested after culturing hBMSCs on the TiR and TiS surfaces for 7 days. MiRNA expression profiling was performed using Agilent miRNA microarrays version 2.2 according to the manufacturer's protocol (Capitalbio Technology, Beijing, China). The potential miRNAs were selected from differentially expressed miRNAs according to the cell skeleton, morphology, and cell differentiation functions of gene targets using prediction website including TargetScan and miRDB.

2.5. MiRNA transfection

The mimic and mimic control (mimic-NC) of miRNAs were separately transfected at 50 nM. The inhibitor and inhibitor control (inhibitor-NC) of miRNAs were separately transfected at 100 nM using Lipofectamine 3000 (Thermo Fisher Scientific, Invitrogen, Waltham, MA, USA) according to the manufacturer's instructions. After 72 h of transfection, all cells were harvested for related mRNA and protein analyses. The RNA oligoribonucleotides used as mimics, inhibitors, mimic-NCs, and inhibitor-NCs were purchased from RiboBio (Guangzhou, China).

2.6. RNA purification and gene expression analyses

The hBMSCs were cultured on TiR and TiS slices in 6-well plates with standard growth medium or osteogenic induction medium; the medium was changed every 2 days. Total RNA was extracted utilizing a total isolation kit after 7 days of cultivation (RNeasy Plus Mini Kit; Qiagen, Valencia, CA, USA). The levels of runt-related transcription factor 2 (*RUNX2*) and osterix (*OSX*) mRNA expression were determined by qPCR with Power SYBR Green PCR Master Mix and an ABI PRISM 7500 system (BGI, Shenzhen, China). The internal control was glyceraldehyde-3-phosphate (*GAPDH*). For miRNAs, reverse transcription was conducted using the All-in-One™ First-Strand cDNA Synthesis Kit (GeneCopoeia, Guangzhou, China) after extracting total RNA. Then, qPCR was performed to evaluate the differentially expressed miRNAs and osteogenesis-related genes. The relative miRNA expression levels were normalized to the expression of U6 (cat. no. miRAN0002; RiboBio). Forward and reverse primers for the genes are listed in Table S1

(Supplementary Material). Cycle threshold values (Ct values) were used to calculate fold differences by the $2^{-\Delta\Delta Ct}$ method.

2.7. Western blotting

The slices with cultured hBMSCs were washed with ice-cold PBS. The cells were lysed in radioimmunoprecipitation assay (RIPA) lysis buffer (Solarbio). The lysates were sonicated and centrifuged at $12,000 \times g$ for 20 min at 4 °C to obtain total protein. The proteins were separated on 10% SDS-polyacrylamide gels and transferred to a polyvinylidene difluoride membrane (Millipore, Cambridge, MA, USA). The membrane was blocked with 1% BSA for 1 h and incubated with primary antibodies against RUNX2, OSX (Abcam, Cambridge, UK), and GAPDH (BGI, Shenzhen, China) at 4 °C overnight. Then, membranes were incubated with secondary antibodies for 1 h and visualized with an Enhanced Chemiluminescent (ECL) Kit (CoWin Biotech, Beijing, China) at room temperature.

2.8. Alkaline phosphatase (ALP) assays

ALP staining was carried out after osteogenic induction for 7 days. The hBMSCs were fixed in 4% paraformaldehyde for 20 min and washed with PBS. Then, ALP staining was performed using an NBT/BCIP Staining Kit (CoWin Biotech) following the manufacturer's instructions. Moreover, the wells were washed twice with PBS, and ALP activity was determined in the cell lysate using an ALP Kit (Jiancheng, Nanjing, China) after 7 days. The protein content in the cell lysates was analyzed using the BCA Assay Kit (Thermo) and ALP activity was normalized against the total protein concentration.

2.9. Alizarin red (AR) assays

AR staining was conducted after osteogenic induction for 14 days to determine mineralized nodule formation. The cells were fixed in 95% ethanol for 30 min, washed with deionized water, and then stained with 0.1% AR (Sigma-Aldrich) for 1 h at room temperature. To quantitatively assess the mineralization degree, the stained mineralized nodules were dissolved in 10% cetylpyridinium chloride for 1 h and the absorbance of solution was detected at 570 nm.

2.10. Luciferase assay

The luciferase reporter plasmids containing the wild type (pEZX-MT05-Wild type) or a mutant fragment of target gene (pEZX-MT05-mutant) were constructed by GeneCopoeia. 293T cells were cultured in 12-well plates at a density of 1×10^5/well. As the confluence of cells reaching to 50–70%, 293T cells were co-transfected with the plasmids and the miRNA mimic or mimic-NC oligonucleotide using Lipofectamine 3000. After transfection for 48 h, the supernatant was collected and GLuc/SEAP activity was measured using a Secrete-Pair Dual Luminescence Assay Kit (GeneCopoeia).

2.11. Statistical analysis

All statistical analyses were performed with Prism 7.0 (GraphPad Software, CA, USA). Data are expressed as the means ± standard deviation of three repeated experiments. Student's *t*-tests were used to compare the differences between two groups. A two-tailed *p*-value <0.05 was considered statistically significant.

3. Results and discussion

3.1. Implant surfaces with moderate roughness enhance osteogenic differentiation of hBMSCs

The topography of the TiR and TiS surfaces were characterized by

SEM and a 3D optical profiler. SEM showed that micro-nano hierarchical ridges with various size pores were observed on the TiR surface and some milled traces were observed on the flat TiS surface (Fig. 1a). The 3D optical profiler showed no orientation on TiR and a clear orientation on TiS (Fig. 1b). Based on the surface roughness parameters Sa and Sq, the TiR surface (Sa: 1.858 ± 0.005 μm, Sq: 2.395 ± 0.007 μm) was obviously rougher than the TiS surface (Sa: 0.222 ± 0.007 μm, Sq: 0.279 ± 0.013 μm; $p < 0.05$; Fig. 1c, d).

The fluorescent images (Fig. 1e) showed that the cells cultured on TiS surface appeared flatted with convex edges. The actin filaments were mostly distributed within the cells and stress fibers were arrayed along the main directions of tensional force. In comparison, the morphology of cells on TiR surface exhibited a stellate shape with concave edges and abundant filopodia. The cells have more stress fibers along the outer edge and with the filopodia [23,24]. A review summarized that the cells have a distinctly different morphology on various surfaces. The cells are less well spread on rougher surface and attached to the surface through cytoplasmic extensions. This rearrangement of the cytoskeleton can transduce information about the surface to nucleus [25]. The CCK-8 assay revealed that the cell proliferation was decreased with surface roughness increased, which are consistent with previous observations [26,27]. There were no significant differences in cell proliferation between two groups after culturing for 1 day, while the cell proliferation culture on rough surface lower that on smooth surface after culturing for 3 and 7 days (Fig. S1, Supplementary Material).

The osteogenic differentiation of hBMSCs was evaluated after 7 days of cultivation. In the ALP staining images, blue-stained hBMSCs observed on TiR surface were more prevalent than those on the TiS surface (Fig. 1f). Quantitative ALP activity analyses also showed that ALP levels in the TiR group were higher than in those in the TiS group ($p < 0.05$; Fig. 1g). Moreover, qPCR indicated that *RUNX2* and *OSX* mRNA expression levels in hBMSCs on the TiR surface were both higher than those on the TiS surface ($p < 0.05$; Fig. 1h, i). The topographical features of implant surfaces can orchestrate stem cell differentiation via cellular mechanotransduction [28]. Surface topography is determined by surface roughness and orientation. Whether a surface is isotropic or anisotropic, however, seems to be of little importance for implants inserted into bone, as reported previously [14]. Thus, the diverse osteogenic differentiation observed in TiR and TiS was mainly influenced by surface roughness. These results confirmed that the TiR surface with moderate roughness had better osteoconductivity than the TiS surface with smooth roughness [16].

3.2. MiRNA expression profiling of changes in hBMSCs cultured on TiR and TiS surfaces and the selection of candidate miRNAs

MiRNA microarray analysis was used to rapidly screen the differentially expressed miRNAs in hBMSCs cultured on TiR and TiS surfaces. The heat map showed the differences in miRNA expression indicated by the color key (Fig. 2a). A scatter plot revealed the differential extent of miRNA expression (Fig. S2, Supplementary Material). There were 13 upregulated miRNAs and 147 downregulated miRNAs on the TiR surfaces compared to levels on the TiS surfaces. Subsequently, twenty-nine potential miRNAs were selected using the prediction software according to the functions of the miRNAs target genes (Table S2, Supplementary Material). The expression levels of the potential miRNAs in hBMSCs cultured on TiR and TiS surfaces were further confirmed by qPCR (Fig. 2b). Consequently, four miRNAs including one upregulated miRNA (miR-5703) and three downregulated miRNAs (miR-1249-5p, miR-181d-5p, and miR-431-3p) were significantly differentially expressed with or without osteogenic induction between the TiR and TiS groups ($p < 0.05$).

To explore whether miR-5703, miR-1249-5p, miR-181d-5p, and miR-431-3p were related to osteogenic differentiation, the relative *RUNX2* levels were investigated by qPCR after transfecting corresponding mimics, mimic-NCs, inhibitors, and inhibitor-NCs in standard
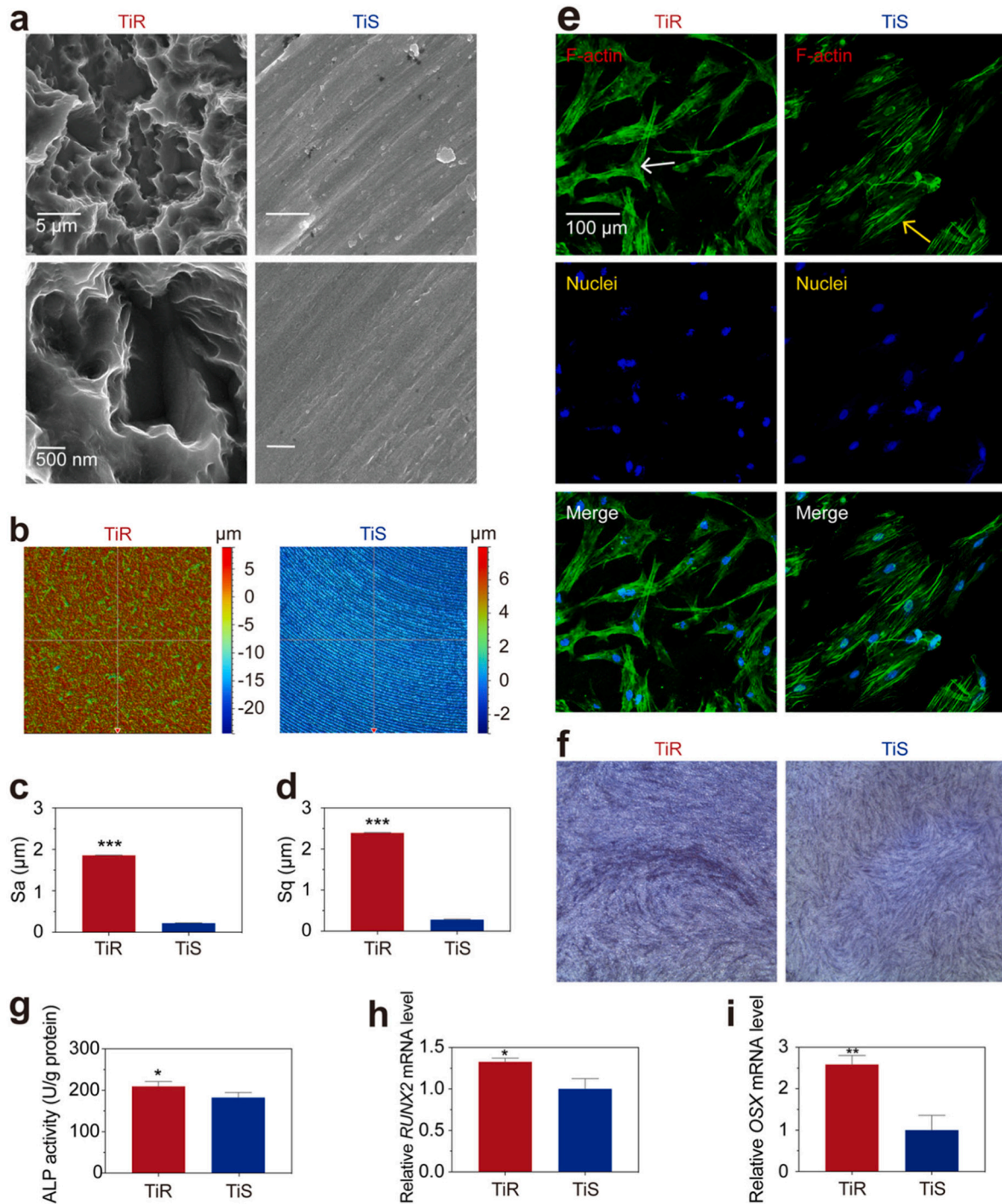
Fig. 1. Implant surfaces with moderate roughness (TiR) enhance the osteogenic differentiation of human bone marrow stem cells (hBMSCs) compared to that with smooth roughness (TiS). (a) Representative scanning electron microscopy images for the TiR and TiS surfaces. (b) Three-dimensional (3D) morphologies of the TiR and TiS surfaces acquired by a 3D optical profiler. Surface roughness was analyzed by the calculation of 3D parameters including (c) Sa: arithmetic mean deviation of the surface and (d) Sq: root-mean-square deviation of the surfaces. (e) Immunofluorescent images of nuclei stained with 4′,6-diamidino-2-phenylindole (DAPI), F-actin stained with FITC-labeled phalloidin, and merged images of hBMSCs on TiR and TiS surfaces. White arrow indicating concave edges, yellow arrow indicating convex edges. (f) Alkaline phosphatase activity (ALP) staining of the hBMSCs on the TiR and TiS surfaces. (g) Quantitative ALP activity was normalized against the total protein concentration. (h) Relative *RUNX2* and (i) *OSX* mRNA expression levels. $*p < 0.05$, $**p < 0.01$, $***p < 0.001$. (For interpretation of the references to color in this figure legend, the reader is referred to the web version of this article.)

medium or osteogenic induction medium. The expression of miR-5703 was increased by more than 100-fold in the mimic group compared to that in the mimic-NC group and was decreased by approximately 70% in the inhibitor group compared to that in the inhibitor-NC group (Fig. 2c). There were no statistical differences in relative *RUNX2* mRNA expression levels between miR-5703-mimic and mimic-NC groups without

osteogenic induction and between miR-5703-inhibitor and inhibitor-NC groups with or without osteogenic induction ($p > 0.05$). The *RUNX2* levels in the miR-5703-mimic group were higher than those in the mimic-NC group with osteogenic induction ($p < 0.05$; Fig. 2d). The miR-1249-5p expression was increased by approximately 25-fold in the mimic group and reduced by half in the inhibitor group (Fig. 2e). There
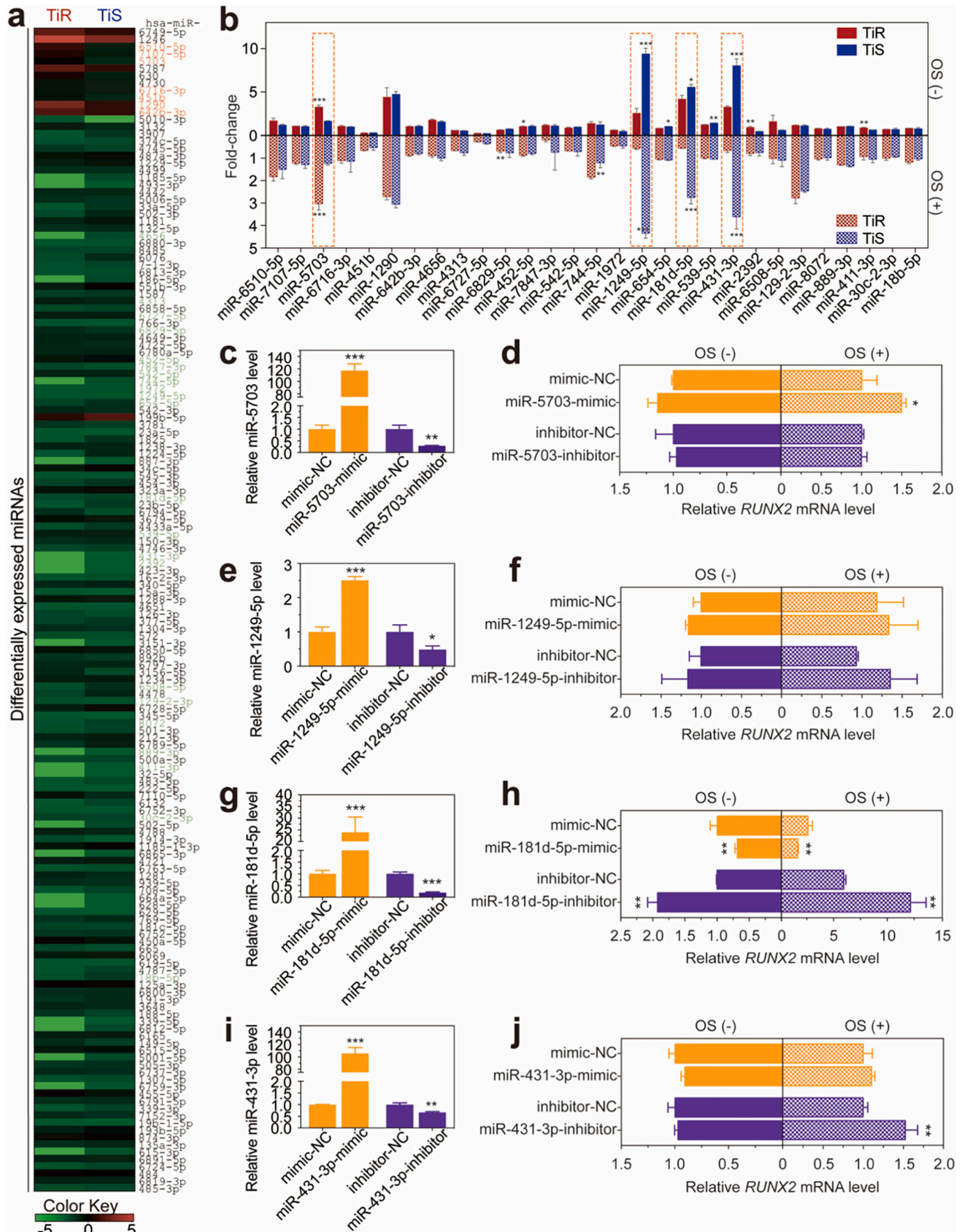
(caption on next page)

Fig. 2. MiRNA selection processes. (a) Heat-map of the differentially expressed miRNAs in the human bone marrow stem cells (hBMSCs) cultured on the smooth roughness (TiS) and moderate roughness (TiR) surfaces. (b) The expression levels of potential miRNAs on TiS and TiR surfaces. Relative miRNA expression levels after the transfection of mimics, mimic-NCs, inhibitors, and inhibitor-NCs for (c) miR-5703, (e) miR-1249-5p, (g) miR-181d-5p, and (i) miR-431-3p. Relative *RUNX2* mRNA expression levels after the transfection of mimics, mimic-NCs, inhibitors, and inhibitor-NCs for (d) miR-5703, (f) miR-1249-5p, (h) miR-181d-5p, and (j) miR-431-3p. OS (−) indicate standard medium, OS (+) osteogenic induction medium. *$p < 0.05$, **$p < 0.01$, ***$p < 0.001$. (For interpretation of the references to color in this figure, the reader is referred to the web version of this article.)

were neither statistical differences in *RUNX2* levels between miR-1249-5p-mimic and mimic-NC groups, nor statistical differences in that between miR-1249-5p-inhibitor and inhibitor-NC groups with or without osteogenic induction (Fig. 2f; $p > 0.05$). The expression of miR-181d-5p was increased by more than two-fold in the overexpression group and decreased by approximately 50–80% in the knockdown group (Fig. 2g). Notably, the overexpression of miR-181d-5p inhibited the relative *RUNX2* mRNA expression levels, whereas the suppression of miR-181d-5p had opposite effects on *RUNX2* expression (Fig. 2h; $p < 0.01$). The miR-431-3p expression was enhanced by more than 100-fold in the mimic group and decreased by approximately 40% in the inhibitor group (Fig. 2i). *RUNX2* mRNA expression levels between miR-431-3p-inhibitor and inhibitor-NC groups exhibited statistical differences under osteogenic induction (Fig. 2j; $p < 0.01$).

After stepwise selection, miR-181d-5p was selected for in-depth studies as it was closely correlated with the osteogenic differentiation of hBMSCs. MiR-181s have key roles in cell differentiation and cell fate [29–31]. The miR-181 family consists of six mature miRNAs (i.e. miR-181a1, miR-181a2, miR-181b1, miR-181b2, miR-181c, and miR-181d) were encoded in three independent transcripts on three separate chromosomes [32]. During early hematopoiesis, miR-181a is upregulated in differentiated B-lymphocytes compared with the levels in undifferentiated progenitor cells [33]. MiR-181a is overexpressed in the presence of macrophage colony-stimulating factor [34]. MiR-181b and miR-181c are downregulated during megakaryocytic differentiation [35], whereas the overexpression of miR-181a could activate megakaryocytic differentiation by interrupting Lin28 expression and increasing the expression of let-7 [36]. Additionally, strontium directly inhibits osteoclast differentiation by enhancing lipoprotein receptor-related protein 6, β-catenin, and osteoprotegerin, which are targeted by miR-181d-5p [37].

In this study, the related enriched terms and pathways on the two surfaces were also identified by gene ontology (GO; Fig. S3, Supplementary Material) and Kyoto encyclopedia of genes and genomes (KEGG) pathway enrichment analyses (Fig. S4, Supplementary Material). Cytoskeletal organization and cell to cell junction were enriched on the moderately rough surface. The key pathways related to the surface roughness, including osteogenic-related activities, such as focal adhesion, the MAPK signaling pathway, and the Wnt signaling pathway, were also enhanced on the moderately rough surface. Previous studies demonstrated that the surface roughness affects cell osteogenic differentiation by changing cell behaviors, such as altering protein synthesis, cell spreading, adhesion, and proliferation in response to mechanical forces [7,38–40]. The osteogenic regulation of focal adhesion in stem cells in the material microenvironment involves initial integrin binding to extracellular matrix components and the reinforcement of the adhesion plaques through further protein recruitment [41]. Various surface topographies enhance osteogenesis via the activation of MAPK signaling [42,43] or Wnt signaling [44,45]. The network interactions between cellular signaling pathways and miRNAs triggered by surface characteristics of roughness deserve further investigation for the development of implant materials.

3.3. Downregulation of miR-181d-5p is correlated with enhanced osteogenic differentiation of hBMSCs

To further verify the roles of miR-181d-5p in the biophysical and chemical stimuli of osteogenic differentiation of hBMSCs, qPCR, western

blotting, ALP tests, and AR tests were performed with standard growth medium and osteogenic induction medium (Fig. 3). The overexpression and suppression of miR-181d-5p in hBMSCs, respectively, inhibited and enhanced the relative *OSX* mRNA expression levels with or without osteogenic induction ($p < 0.01$; Fig. 3a). The protein expression levels of RUNX2 and OSX were downregulated when miR-181d-5p was overexpressed in hBMSCs with or without osteogenic induction but were upregulated when miR-181d-5p was knocked down (Fig. 3b). Additionally, ALP staining and ALP quantitative experiments showed that ALP activity in the miR-181d-5p knockdown group was higher than that in the control group, but ALP activity in the miR-181d-5p overexpressed group was lower than that in the control group after cultivation for 7 days with or without osteogenic induction ($p < 0.05$; Fig. 3c, d). As hBMSCs were cultured in osteogenic inductive medium, the intensity of AR staining was significantly higher in the miR-181d-5p knockdown group than in the control group, indicating that matrix mineralization was increased after cultivation for 14 days, and this was lower in the miR-181d-5p overexpressed group than in the control group ($p < 0.001$). When hBMSCs were cultured in standard growth medium, the intensity of AR staining in miR-181d-5p-mimic, mimic-NC, miR-181d-5p-inhibitor, and inhibitor-NC groups was low, but matrix mineralization in the miR-181d-5p-mimic group was lower than that in the mimic-NC groups, whereas this was increased in the miR-181d-5p-inhibitor groups compared to that in the inhibitor-NC group ($p < 0.001$; Fig. 3c, e). The potentially target genes of miR-181d-5p were predicted according to TargetScan and miRDB. MAPK1 is one of target gene of miR-181d-5p with conserved binding site (NM_002745, Fig. 3f). The luciferase reporter activity of the pEZX-MT05-MAPK1-WT/miR-181d-5p was significantly lower than that of the pEZX-MT05-MAPK1-WT/mimics NC. No significant differences were found between pEZX-MT05-MAPK1-mut/miR-181d-5p and pEZX-MT05-MAPK1-mut/mimics NC (Fig. 3g). The luciferase assay result suggested that the miR-181d-5p targeted the 3′-UTR of MAPK1. As previous studies reported, MAPK pathway played an important role in regulating the activity and function of RUNX2 for osteogenic differentiation and bone information [46,47].

Cell responses to mechanical stimuli involve the perception and transmission of signals and subsequent changes in downstream biochemical reactions [48]. During the process of osteogenesis, the biochemical culture environment induces osteogenic differentiation along with gene expression changes prior to cytoskeleton rearrangement and alterations in cell morphology [49], whereas biophysical stimulation induces osteogenic differentiation with changes in focal adhesion and the rearrangement of the cytoskeleton before any changes in gene expression [50]. To investigate the effect of cytoskeletal organization on the expression of miR-181d-5p, the hBMSCs cultured on rough surface were treated with the Rho kinase inhibitor Y27632 which control the cytoskeletal dynamics and gene expression [51]. The results showed that the difference of cell morphology was eliminated, the cytoskeleton of cells on two surfaces were disturbed (Fig. S5a, Supplementary Material), and the difference of miR-181d-5p expression in hBMSCs on two surfaces was diminished (Fig. S5c, Supplementary Material). These data indicated that the variation in miR-181d-5p expression might contribute to the cell morphological differences between two surfaces. Additionally, previous studies demonstrated miR-181d-5p can inhibit cell proliferation [52,53]. This is opposite to our results (i.e. on rough surface, cells proliferated slower with downregulated miR-181d-5p), indicating miR-181d-5p is not the main regulator for cell proliferation in this study. The expression miR-181d-5p is also influenced by chemical stimuli in
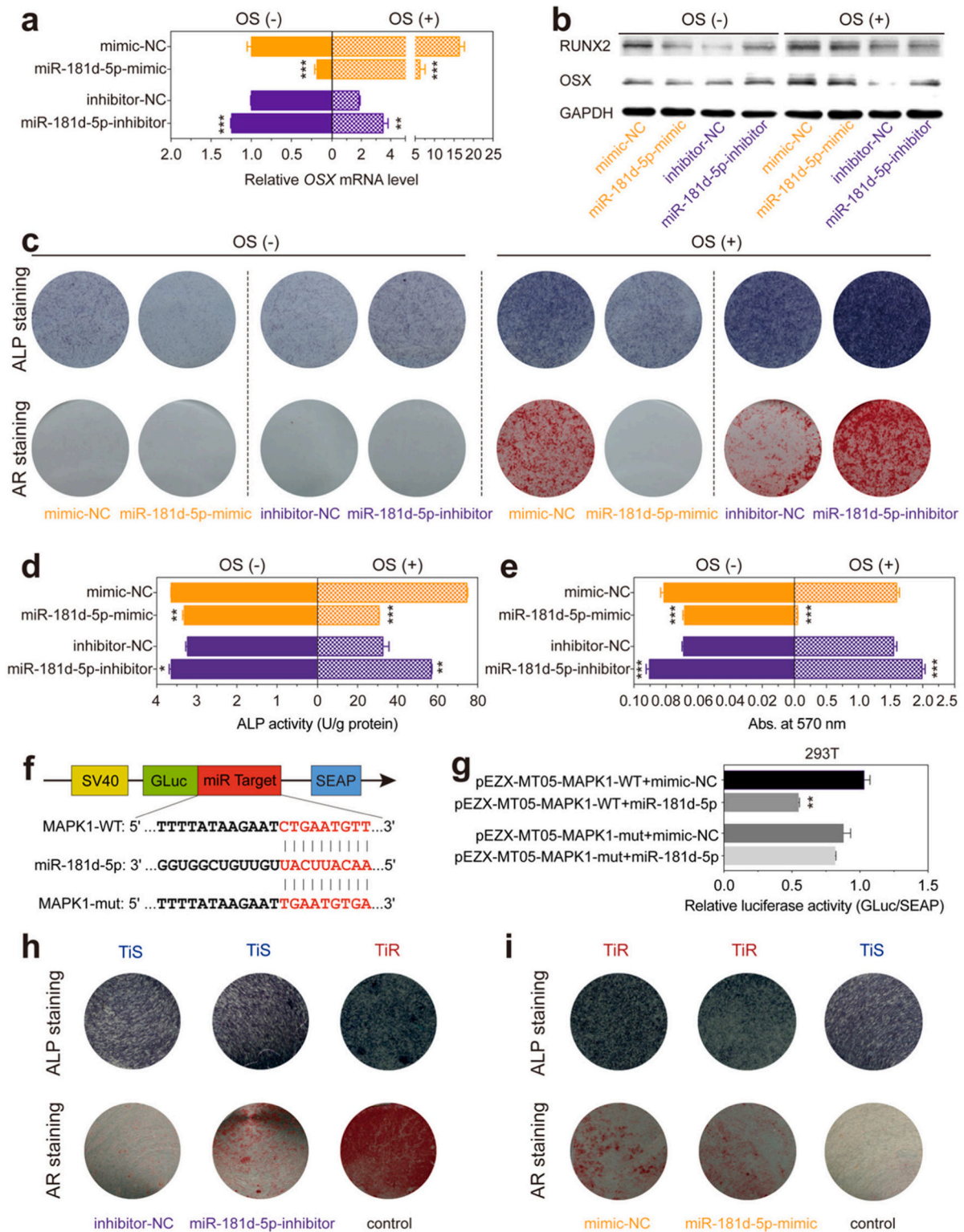
Fig. 3. Downregulation of miR-181d-5p in human bone marrow stem cells (hBMSCs) enhances osteogenic differentiation. (a) Relative *OSX* mRNA expression levels after the transfection of mimic, inhibitor, and inhibitor-NC for miR-181d-5p. (b) Effects of miR-181d-5p-mimic, mimic-NC, miR-181d-5p-inhibitor, and inhibitor-NC on RUNX2 and OSX expression at the protein level. (c) Alkaline phosphatase (ALP) staining, (d) ALP normalized protein levels, alizarin red (AR) staining and (e) quantitative AR evaluation of the mineralized nodules of hBMSCs transfected with miR-181d-5p-mimic, miR-181d-5p-inhibitor, and the corresponding controls. (f) The schematic of luciferase reporter plasmids containing the 3′-UTR of wild type or mutant MAPK1. (g) Relative luciferase activity. (h) ALP staining and AR staining after transfection with miR-181d-5p-inhibitor or inhibitor-NC in the hBMSCs on smooth roughness (TiS) surface and without transfection in the hBMSCs on the moderate roughness (TiR) surface. (i) ALP staining and AR staining after transfection with miR-181d-5p-mimic or mimic-NC in the hBMSCs on TiR and without transfection in the hBMSCs on TiS. OS (−) indicate standard medium, OS (+) osteogenic induction medium. *$p < 0.05$, **$p < 0.01$, ***$p < 0.001$.

addition to cellular mechanosensing. The expression of miR-181d-5p in the hBMSCs with osteogenic induction was suppressed by approximately 75% on a rough surface and 50% on a smooth surface compared with levels in regular growth medium. Moreover, the differences in osteogenic capacity between the miR-181d-5p-inhibitor and inhibitor control groups were extended due to the addition of osteogenic induction. Therefore, the inhibition of miR-181d-5p induced the osteogenic differentiation triggered by biophysical and biochemical stimuli.

3.4. MiR-181d-5p-inhibitor improves the inferior bone formation on a smooth TiS surface and miR-181d-5p-mimic suppresses the superior bone formation on a rough TiR surface

To evaluate the osteogenic potential of miR-181d-5p-inhibitor, we cultured hBMSCs with miR-181d-5p knocked down on the TiR surface, cultured hBMSCs transfected with inhibitor-NC on the TiS surface, and cultured hBMSCs without transfection on the TiR surface (control). After cultivation for 7 days, weaker staining and fewer ALP-positive cells were observed in the group transfected with inhibitor-NC, but staining and ALP-positive cells in the group with miR-181d-5p knockdown were similar to those of the control group. After cultivation for 14 days, the intensity of AR staining observed in the control group was increased compared to that in the group with miR-181d-5p knockdown, and that in the knockdown group was increased in the group transfected with inhibitor-NC. In other words, hBMSC culture with low miR-181d-5p expression could rescue the effects of early bone resorption on a smooth TiS surface after cultivation for 7 days (Fig. 3h).

The roles of miR-181d-5p-mimic in disrupting bone formation were evaluated by comparing ALP activity and matrix mineralization in cultured hBMSCs overexpressing miR-181d-5p on the TiR surface and hBMSCs without transfection on the TiS surface (control). After cultivation for 7 days, weaker staining and fewer ALP-positive cells were observed in the miR-181d-5p overexpression group than in the mimic-NC and control groups. After cultivation for 14 days, AR staining results showed that the mimic-NC group exhibited increased mineralized nodule formation compared to that in the miR-181d-5p-mimic group. The mineralized nodule formation in the miR-181d-5p-mimic group was similar to that in the control group. These results indicate that high miR-181d-5p expression reduces the osteogenic potential in the TiR group (Fig. 3i). Rescue experiments demonstrated that miR-181d-5p-inhibitor

could induce osteogenesis on a smooth surface and might be applied to the dental implant neck, which always contains a smooth collar to preserve periodontal tissues around the implants; this portion still needs to possess the capacity to promote osteogenesis [54,55].

4. Conclusion

In this study, by applying the smooth titanium surface as a control, a typical titanium surface with moderate roughness was prepared here to reveal the mechanism through which surface roughness regulates cell osteogenic behavior by altering miRNA expression (Schematic 1). We provided evidence that the implant surface with moderate roughness promotes the osteogenic differentiation of hBMSCs compared to that with smooth roughness. MiRNA profiling analyses revealed the differential expression miRNAs between two different surfaces. Four candidate miRNAs were selected after the prediction of gene target function and verification by qPCR. Overexpression and knockdown experiments based on the four candidate miRNAs suggested that only miR-181d-5p is closely correlated with osteogenic gene expression. We further confirmed that the downregulation of miR-181d-5p promotes the osteogenic differentiation of hBMSCs, and vice versa, based on osteogenesis-related gene and protein expression, as well as alkaline phosphatase and alizarin red experiments. Additionally, the rescue assay results indicated that the knockdown of miR-181d-5p could improve the inferior osteogenesis on smooth surfaces, whereas the overexpression of miR-181d-5p suppressed the superior osteogenesis on rough surfaces. These results improve our understanding of mechanisms through which implant surface roughness determines stem cell function and fate at the molecular level and provide helpful information and a theoretical basis for the development of implant materials for fast osteointegration.

CRediT authorship contribution statement
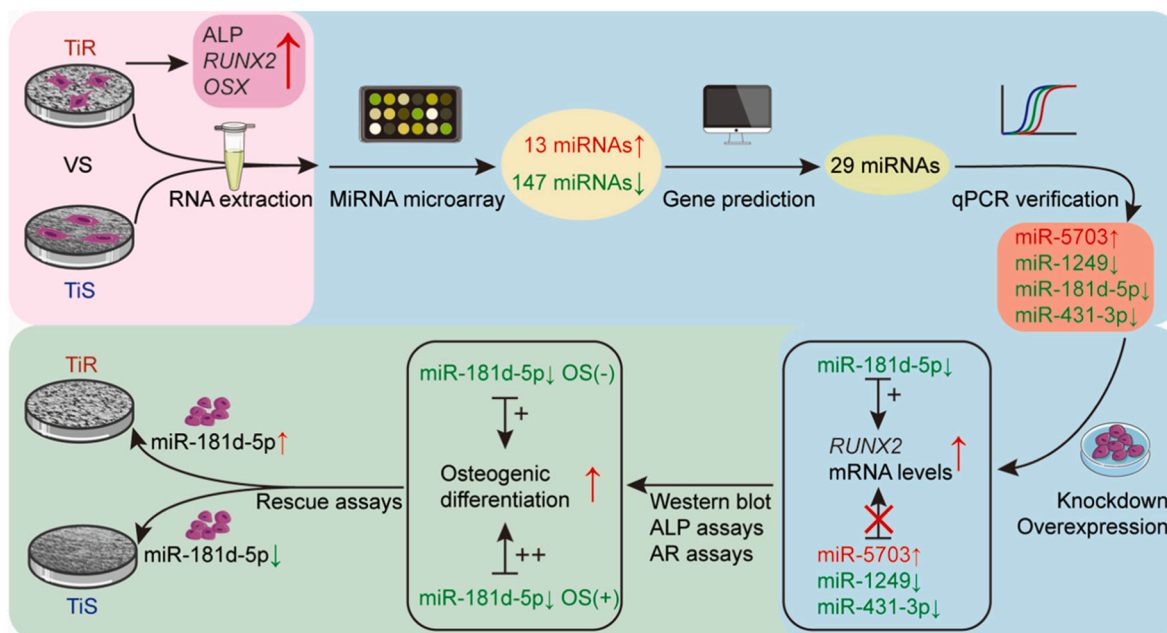
Schematic 1. Overview of the study.

Declaration of competing interest

The authors declare that they have no known competing financial interests or personal relationships that could have appeared to influence the work reported in this paper.

Acknowledgments

Appendix A. Supplementary data

Supplementary data to this article can be found online at https://doi.org/10.1016/j.msec.2020.111801.

References

[1] D. Bian, J. Deng, N. Li, X. Chu, Y. Liu, W. Li, H. Cai, P. Xiu, Y. Zhang, Z. Guan, ACS Appl. Mater. Interfaces 10 (2018) 4394–4408.
[2] S. Mishinov, V. Stupak, N. Koporushko, A. Samokhin, A. Panchenko, I. Krasovskii, I. Desyatykh, A. Kiselev, Biomed. Eng. 52 (2018) 152–155.
[3] J. Yeung, A. Griffin, S. Newton, M. Kenna, G.R. Licameli, Laryngoscope 128 (2018) 2619–2624.
[4] G. Wang, X. Gao, E.C. Lo, J. Dent. 43 (2015) 798–805.
[5] F.A. Shah, P. Thomsen, A. Palmquist, Acta Biomater. 84 (2019) 1–15.
[6] S.B. Goodman, Z. Yao, M. Keeney, F. Yang, Biomaterials 34 (2013) 3174–3183.
[7] D.D. Deligianni, N.D. Katsala, P.G. Koutsoukos, Y.F. Missirlis, Biomaterials 22 (2000) 87–96.
[8] D. Buser, N. Broggini, M. Wieland, R. Schenk, A. Denzer, D.L. Cochran, B. Hoffmann, A. Lussi, S. Steinemann, J. Dent. Res. 83 (2004) 529–533.
[9] T. Albrektsson, P.-I. Brånemark, H.-A. Hansson, J. Lindström, Acta Orthop. Scand. 52 (1981) 155–170.
[10] D.A. Fletcher, R.D. Mullins, Nature 463 (2010) 485–492.
[11] G. Abagnale, M. Steger, V.H. Nguyen, N. Hersch, A. Sechi, S. Joussen, B. Denecke, R. Merkel, B. Hoffmann, A. Dreser, Biomaterials 61 (2015) 316–326.
[12] M. Glibert, C. Matthys, R.J. Maat, H. De Bruyn, S. Vervaeke, Clin. Implant. Dent. Relat. Res. 20 (2018) 824–828.
[13] B.A. Van Oirschot, R.M. Eman, P. Habibovic, S.C. Leeuwenburgh, Z. Tahmasebi, H. Weinans, J. Alblas, G.J. Meijer, J.A. Jansen, J.J. Van Den Beucken, Acta Biomater. 37 (2016) 195–205.
[14] A. Wennerberg, T. Albrektsson, Clin. Oral Implants Res. 20 (2009) 172–184.
[15] M. Hasegawa, J. Saruta, M. Hirota, T. Taniyama, Y. Sugita, K. Kubo, M. Ishijima, T. Ikeda, H. Maeda, T. Ogawa, Int. J. Mol. Sci. 21 (2020) 783.
[16] A.L. Rosa, M.M. Beloti, Clin. Oral Implants Res. 14 (2003) 43–48.
[17] K. Vandamme, I. Naert, J. Vander Sloten, R. Puers, J. Duyck, J. Periodontol. 79 (2008) 150–157.
[18] V. Ambros, Nature 431 (2004) 350–355.
[19] D.P. Bartel, Cell 116 (2004) 281–297.
[20] J. Huang, L. Zhao, L. Xing, D. Chen, Stem Cells 28 (2010) 357–364.
[21] M.Q. Hassan, J.A. Gordon, M.M. Beloti, C.M. Croce, A.J. Van Wijnen, J.L. Stein, G. S. Stein, J.B. Lian, Proc. Natl. Acad. Sci. 107 (2010) 19879–19884.
[22] Y. Lv, Y. Huang, M. Xu, B.C. Heng, C. Yang, C. Cao, Z. Hu, W. Liu, X. Chi, M. Gao, Advanced Science 7 (2020) 1901412.
[23] C. Galli, M. Piemontese, S. Lumetti, F. Ravanetti, G. Macaluso, G. Passeri, Acta Biomater. 8 (2012) 2963–2968.
[24] P.S. Mathieu, E.G. Loboa, Tissue Eng. B Rev. 18 (2012) 436–444.
[25] B.D. Boyan, C.H. Lohmann, D.D. Dean, V.L. Sylvia, D.L. Cochran, Z. Schwartz, Annu. Rev. Mater. Res. 31 (2001) 357–371.
[26] B.D. Boyan, T.W. Hummert, D.D. Dean, Z. Schwartz, Biomaterials 17 (1996) 137–146.
[27] A.L. Rosa, M.M. Beloti, Braz. Dent. J. 14 (2003) 16–21.
[28] T. Luo, K. Mohan, P.A. Iglesias, D.N. Robinson, Nat. Mater. 12 (2013) 1064–1071.
[29] I. Naguibneva, M. Ameyar-Zazoua, A. Polesskaya, S. Ait-Si-Ali, R. Groisman, M. Souidi, S. Cuvellier, A. Harel-Bellan, Nat. Cell Biol. 8 (2006) 278–284.
[30] N.M. Kane, L. Howard, B. Descamps, M. Meloni, J. McClure, R. Lu, A. McCahill, C. Breen, R.M. Mackenzie, C. Delles, Stem Cells 30 (2012) 643–654.
[31] C. Braicu, D. Gulei, L. Raduly, A. Harangus, A. Rusu, I. Berindan-Neagoe, Mol. Asp. Med. 70 (2019) 90–105.
[32] J. Ji, T. Yamashita, A. Budhu, M. Forgues, H.L. Jia, C. Li, C. Deng, E. Wauthier, L. M. Reid, Q.H. Ye, Hepatology 50 (2009) 472–480.
[33] C.-Z. Chen, L. Li, H.F. Lodish, D.P. Bartel, Science (New York, N.Y.) 303 (2004) 83–86.
[34] H. Li, T. Jiang, M.-Q. Li, X.-L. Zheng, G.-J. Zhao, Front. Immunol. 9 (2018) 1175.
[35] R. Garzon, F. Pichiorri, T. Palumbo, R. Iuliano, A. Cimmino, R. Aqeilan, S. Volinia, D. Bhatt, H. Alder, G. Marcucci, Proc. Natl. Acad. Sci. 103 (2006) 5078–5083.
[36] X. Li, J. Zhang, L. Gao, S. McClellan, M. Finan, T. Butler, L. Owen, G. Piazza, Y. Xi, Cell Death Differ. 19 (2012) 378–386.
[37] T. Sun, Z. Li, X. Zhong, Z. Cai, Z. Ning, T. Hou, L. Xiong, Y. Feng, F. Leung, W. W. Lu, Journal of Cell Communication and Signaling 13 (2019) 85–97.
[38] E.G. Long, M. Buluk, M.B. Gallagher, J.M. Schneider, J.L. Brown, Bioactive Materials 4 (2019) 249–255.
[39] D.D. Deligianni, N. Katsala, S. Ladas, D. Sotiropoulou, J. Amedee, Y. Missirlis, Biomaterials 22 (2001) 1241–1251.
[40] R.A. Gittens, T. McLachlan, R. Olivares-Navarrete, Y. Cai, S. Berner, R. Tannenbaum, Z. Schwartz, K.H. Sandhage, B.D. Boyan, Biomaterials 32 (2011) 3395–3403.
[41] W. Wang, L. Zhao, K. Wu, Q. Ma, S. Mei, P.K. Chu, Q. Wang, Y. Zhang, Biomaterials 34 (2013) 631–640.
[42] M.J. Biggs, R.G. Richards, N. Gadegaard, C.D. Wilkinson, R.O. Oreffo, M.J. Dalby, Biomaterials 30 (2009) 5094–5103.
[43] C. Ge, G. Xiao, D. Jiang, R.T. Franceschi, J. Cell Biol. 176 (2007) 709–718.
[44] W. Wang, L. Zhao, Q. Ma, Q. Wang, P.K. Chu, Y. Zhang, Biomaterials 33 (2012) 7993–8002.
[45] G. Li, Y. Song, M. Shi, Y. Du, W. Wang, Y. Zhang, Acta Biomater. 49 (2017) 235–246.
[46] T. Saito, K. Nishida, T. Furumatsu, A. Yoshida, M. Ozawa, T. Ozaki, Osteoarthr. Cartil. 21 (2013) 165–174.
[47] D. Zhang, D. Liu, J. Zhang, C. Fong, M. Yang, Mater. Sci. Eng. C 42 (2014) 70–77.
[48] A.R. Bausch, U.S. Schwarz, Nat. Mater. 12 (2013) 948–949.
[49] R. Fraioli, K. Dashnyam, J.-H. Kim, R.A. Perez, H.-W. Kim, J. Gil, M.-P. Ginebra, J. M. Manero, C. Mas-Moruno, Acta Biomater. 43 (2016) 269–281.
[50] G. Abagnale, A. Sechi, M. Steger, Q. Zhou, C.-C. Kuo, G. Aydin, C. Schalla, G. Müller-Newen, M. Zenke, I.G. Costa, Stem Cell Reports 9 (2017) 654–666.
[51] Z. Chen, X. Wang, Y. Shao, D. Shi, T. Chen, D. Cui, X. Jiang, Mol. Cell. Biochem. 358 (2011) 221–227.
[52] H. Chen, Z. Xiao, R. Yu, Y. Wang, R. Xu, X. Zhu, Biochem. Biophys. Res. Commun. 503 (2018) 1434–1441.
[53] Y. Zhang, C. Li, C. Guan, B. Zhou, L. Wang, C. Yang, L. Zhen, J. Dai, L. Zhao, W. Jiang, Front. Physiol. 11 (2020).
[54] M. Peñarrocha-Diago, A. Flichy-Fernández, R. Alonso-González, D. Peñarrocha-Oltra, J. Balaguer-Martínez, M. Peñarrocha-Diago, Clin. Oral Implants Res. 24 (2013) 1192–1200.
[55] E.A. Bratu, M. Tandlich, L. Shapira, Clin. Oral Implants Res. 20 (2009) 827–832.